PERGAMON

International Journal of Solids and Structures 38 (2001) 5833–5845

INTERNATIONAL JOURNAL OF SOLIDS and STRUCTURES

www.elsevier.com/locate/ijsolstr

Dynamic spherical cavity expansion in brittle ceramics

Sikhanda Satapathy *

Institute for Advanced Technology, The University of Texas at Austin, 3925 W. Braker Lane, Suite 400, Austin, TX 78759-5316, USA

Received 28 June 1999; in revised form 19 October 2000

Abstract

In this paper we derived the pressure required to open a spherical cavity in an infinite brittle ceramic at a constant speed. The ceramic material is assumed to crack upon reaching its elastic limit. Subsequent failure of the cracked material due to compressive failure renders pulverization of the material. The pulverized material is assumed to follow a Mohr–Coulomb type constitutive behavior. The results show that at high cavity expansion speeds the comminuted region outruns the cracked region, i.e. the cracked region disappears. At very high cavity expansion speeds the comminuted zone propagation speed saturates at a level slightly below the longitudinal wave speed. Limited comparison with experimental penetration resistance shows reasonable agreement between theory and experiment.

Keywords: Cavity expansion; Penetration resistance; Brittle materials; Armor ceramics; Cracking and comminution; Similarity transformation

1. Introduction

Ceramic materials such as Al_2O_3, AlN, TiB_2, Si_2O_3 etc. hold advantage in many applications over conventional metals due to their low density and high compressive strength. However, since these materials are extremely weak in tension, extensive fracturing and pulverization occurs when subjected to high levels of stresses. Cavity expansion analysis is of interest in various applications such as high-speed penetration, underground explosion, deep punching, design of protective structures against blast loading, impact cratering etc. While quasi-static analyses have been used for deep-punching problems in elastic–plastic materials (Bishop et al., 1945; Wright et al., 1992; Satapathy and Bless, 2000a), dynamic analyses have been developed (Forrestal, 1986; Forrestal and Luk, 1988; Forrestal and Tzou, 1997; Satapathy et al., 1999) for high-speed penetration problems in rocks, metals, concrete, and glass, respectively. The analysis of dynamic response of brittle ceramics is somewhat complicated due to presence of tensile cracking and comminution (breaking into powder like structure). The cavity expansion analysis technique has been extended to ceramic materials by Forrestal and Longcope (1990) and Satapathy and Bless (1996) for quasi-static conditions. Using quasi-static analysis, Satapathy and Bless (2000b) explained the interface defeat phenomena

* Tel.: +1-512-232-4455; fax: +1-512-471-9096.
E-mail address: sikhanda@iat.utexas.edu (S. Satapathy).

0020-7683/01/$ - see front matter
PII: S0020-7683(00)00388-7

Nomenclature

a	radial location of comminuted-cracked boundary	α	C_c/C_e
		$\bar{\alpha}$	$6\lambda_1/(3+4\lambda_1)$
b	radial location of elastic–undisturbed boundary	β	C_p/C_{cr}
		δ	C_p/V
c	radial location of cracked–elastic boundary	δ_1	ratio of saturated zone propagation speed to cavity expansion speed
C_c	speed of the cracked zone boundary	γ	C_c/C_p
C_{cr}	bar wave speed	η	volumetric strain
C_e	dilatational elastic wave speed	λ_1	pressure–shear slope of comminuted material
C_p	speed of the comminuted zone boundary	ν	poisson's ratio
E	Young's modulus	ρ	density
h	radial location of the cavity surface	σ_f	tensile failure strength
P_c	cavity expansion pressure	σ_r	radial stress
r	radial position	σ_θ	hoop stress
R_t	penetration resistance	τ	saturated shear strength of comminuted material
t	time variable	ξ_1	$r/C_c t$, non-dimensional radial location in elastic region
u	particle speed in comminuted region		
u_1	$u/C_c t$, non-dimensional displacement in elastic region	ξ_2	$r/C_c t$, non-dimensional radial location in cracked region
u_2	$u/C_p t$, non-dimensional displacement in cracked region	ξ_3	r/Vt, non-dimensional radial location in comminuted region
u_3	u/Vt, non-dimensional displacement in comminuted region	U	u/V, non-dimensional particle speed in comminuted region
V	cavity expansion velocity		
Y	compressive strength		

in confined armor ceramics. Here we present the dynamic cavity expansion solution to determine the dynamic response of ceramic materials when subjected to cavity expansion at a constant velocity. We adopt the similarity transform method used by Forrestal and Luk (1988) for metals and by Forrestal and Tzou (1997) for concrete material. As an application, we apply the analysis to model high-speed penetration into ceramic targets.

2. Response regions

As discussed by Satapathy and Bless (1996, 2000b), the response region in ceramics due to sudden expansion of a cavity consists of five distinct zones: cavity, comminuted zone, radially cracked zone, elastic zone and undisturbed zone. As the cavity is subjected to an instantaneous expansion velocity, an elastic wave spreads out at the bulk sound speed. The hoop stresses in the elastic region are tensile. Since the tensile strength of the material is very low, radial cracks appear when the hoop stresses equal the tensile strength of the material. The material in the cracked zone can support only compressive radial stress. When the radial stress in cracked ceramic rises to the compressive strength of the material, we assume that the radially cracked material cracks further, and is reduced to a powder (comminuted) like structure. The comminuted material is taken to behave as a Mohr–Coulomb material with zero cohesive strength. Plate

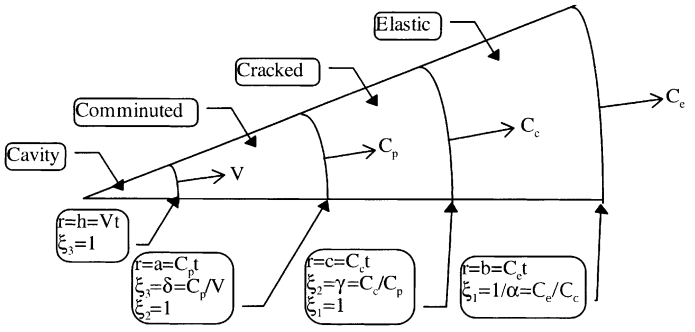

Fig. 1. Dynamic response regions in a spherical cavity.

impact experiments by Rosenberg et al. (1987) have shown that the extensively fractured ceramics can support only a finite amount of shear stress. We examine the implication of 'capping' the Mohr–Coulomb behavior with a constant shear strength. In absence of a better rationality, we assume that the comminuted region is non-dilatant.

Fig. 1 shows the different response regions and designates the boundaries in terms of variables to be introduced in subsequent sections. For spherical symmetry the conservation equations for mass and momentum in Eulerian coordinates are as follows:

$$\frac{\partial \rho}{\partial t} + \frac{1}{r^2}\frac{\partial}{\partial r}(\rho r^2 v) = 0, \tag{1}$$

$$\frac{\partial \sigma_r}{\partial r} + 2\frac{(\sigma_r - \sigma_\theta)}{r} = -\rho\left(\frac{\partial v}{\partial t} + v\frac{\partial v}{\partial r}\right). \tag{2}$$

The stresses are taken to be positive in compression. These two equations have to be integrated in different zones along with the constitutive equations and the boundary conditions to yield the field solutions for the stresses and deformation. Solution of these coupled differential equations is simplified by transforming them by a similarity transformation which reduces the partial differential equations into ordinary differential equations. This method is particularly attractive for applications in penetration problems since it is known that the steady state regime dominates the penetration process for high-velocity penetration. As a result, the associated cavitation phenomenon is self-similar and takes place at a steady velocity for most of the penetration.

3. Elastic region

The stress–displacement relations for spherical symmetry can be written as

$$\sigma_r = -\frac{E}{(1+v)(1-2v)}\left[(1-v)\frac{\partial u}{\partial r} + 2v\frac{u}{r}\right], \tag{3}$$

$$\sigma_\theta = -\frac{E}{(1+v)(1-2v)}\left[v\frac{\partial u}{\partial r} + \frac{u}{r}\right], \tag{4}$$

where stresses are assumed positive in compression. Since the particle velocity in the elastic region is likely to be negligible, we ignore the convective term in Eq. (2). Thus substituting the strain–displacement relations in conservation equations, one obtains

$$\frac{\partial^2 u}{\partial r^2}+\frac{2}{r}\frac{\partial u}{\partial r}-\frac{2u}{r^2}=\frac{1}{C_e^2}\frac{\partial^2 u}{\partial t^2}, \tag{5}$$

where C_e is the dilatational elastic wave speed. Now introducing similarity transformations,

$$\xi_1=\frac{r}{C_c t} \quad \text{and} \quad \bar{u}_1=\frac{u}{C_c t}, \tag{6}$$

Eq. (5) transforms to

$$\frac{d^2\bar{u}}{d\xi_1^2}+\frac{2}{\xi_1}\frac{d\bar{u}}{d\xi_1}-\frac{2\bar{u}}{\xi_1^2}=\alpha^2\xi^2\frac{d^2\bar{u}}{d\xi_1^2}, \tag{7}$$

where $\alpha \equiv C_c/C_e$.

Forrestal and Luk (1988) have shown that Eq. (7) has a solution of the form

$$\bar{u}=A\alpha\xi_1-B\frac{1-3\alpha^2\xi_1^2}{3\alpha^2\xi_1^2}, \tag{8}$$

where A and B are constants of integration to be evaluated from the boundary conditions. We do not envisage the presence of transverse cracks at the elastic–undisturbed interface. Denoting jump in any quantity by double square brackets,

$$\left[\left[\bar{u}\right]\right]_{\xi=1/\alpha}=0, \tag{9}$$

since there is no discontinuity in displacement (hoop cracks) at the elastic–undisturbed boundary. The other boundary condition is given by the fact that the elastic material cracks when the tensile hoop stress equals the tensile strength of the material. That is,

$$\sigma_\theta(\xi_1=1)=-\sigma_f. \tag{10}$$

Using the boundary conditions (9) and (10) in the solution for the transformed displacement solution (Eq. (8)) we get

$$B=-\frac{3}{2}A; \quad A=\left(\frac{\sigma_f}{\frac{1}{2}\rho_0 C_e^2}\right)\frac{\alpha^2(1-\nu)}{2\nu(\alpha^3-1)+(2\alpha^3-3\alpha^2+1)}. \tag{11}$$

4. Cracked region

In this region the hoop stresses are zero due to the presence of radial cracks. For spherical symmetry, the two hoop directions perpendicular to the radial direction are equivalent. The material in this region is then in the form of needles. Alternatively, it is possible that the cracks are distributed in an incoherent and discontinuous manner in such a way that the material cannot support hoop stress and yet is not needle-like. In either case, the material in the cracked region is capable of transmitting only radial stress. Since the hoop stress is zero, Eq. (2) reduces to

$$\frac{\partial\sigma_r}{\partial r}+\frac{2\sigma_r}{r}=-\rho\frac{\partial^2 u}{\partial t^2}. \tag{12}$$

Presence of radial cracks introduces anisotropy in this region and thus we cannot use the isotropic elastic constants. However, absence of transverse cracks ensures no degradation of the elastic moduli in the radial direction. Hence the stress and displacements are related by

$$\sigma_r = -E\frac{\partial u}{\partial r}. \tag{13}$$

For the cracked region we introduce the following similarity transforms,

$$\xi_2 = \frac{r}{C_p t} \quad \text{and} \quad \bar{u}_2 = \frac{u}{C_p t}. \tag{14}$$

Using this similarity transformation and the stress relation, Eq. (13) in the equation of motion (Eq. (12)), we get

$$\frac{d^2\bar{u}_2}{d\xi_2^2} + \frac{2}{\xi_2}\frac{d\bar{u}_2}{d\xi_2} = \beta^2\xi_2^2\frac{d^2\bar{u}_2}{d\xi_2^2}, \tag{15}$$

where $\beta \equiv C_p/C_{cr}; C_{cr} = \sqrt{E/\rho}$, the bar wave speed. Integration of Eq. (15) results in the following expression for the dimensionless displacement in the cracked region:

$$\bar{u}_2 = -c_1\frac{1+\beta^2\xi_2^2}{\xi_2} + c_2, \tag{16}$$

where c_1 and c_2 are constants of integration. The inward boundary of the cracked region is defined by the condition that the cracked material pulverizes when the compressive radial stress exceeds the compressive strength of the material. Thus,

$$\sigma_r(\xi_2 = 1) = -E\frac{d\bar{u}_2}{d\xi_2}\bigg|_{\xi_2=1} = Y. \tag{17}$$

Since no transverse crack is envisaged at the elastic–cracked boundary, the displacement should be continuous there. As a result, we get the second boundary condition for displacement as follows:

$$\bar{u}_2\Big|_{\xi_2=\gamma} = \gamma\bar{u}_1\Big|_{\xi_1=1}, \tag{18}$$

where $\gamma = C_c/C_p$. Evaluating radial stress from Eq. (13) with displacement solution (Eq. (16)) along with the boundary conditions (Eqs. (17) and (18)), we obtain

$$c_1 = \frac{Y}{E(\beta^2-1)} \quad \text{and} \quad c_2 = \frac{Y}{\gamma E}\frac{(\beta^2\gamma^2+1)}{(\beta^2-1)} + \left(\frac{\sigma_f\gamma}{\rho_0 C_e^2}\right)\left[\frac{(1-\nu)(2\alpha^3-3\alpha^2+1)}{2\nu(\alpha^3-1)+(2\alpha^3-3\alpha^2+1)}\right]. \tag{19}$$

5. Hugoniot jump conditions

For the dynamic cavity expansion involving propagation of comminuted, cracked and elastic waves into the undisturbed material, Hugoniot jump conditions have to be satisfied at the propagation front. Denoting quantities on either side of the disturbance by subscripts 1 and 2, Hugoniot jump conditions for mass and momentum can be written as (Courant and Friedrichs, 1948):

$$\rho_1(v_1 - C) = \rho_2(v_2 - C), \tag{20}$$

$$\sigma_2 - \sigma_1 = \rho_1(C - v_1)(v_2 - v_1), \tag{21}$$

where v, C and σ are particle velocity, disturbance velocity and normal stress respectively.

Denoting the volumetric strain by η, i.e.,

$$\eta = \frac{P}{K} = 1 - \frac{\rho_0}{\rho}, \tag{22}$$

Eqs. (20) and (21) can be combined to yield

$$\sigma_+ - \sigma_- = \frac{\rho_0 (C - v_-)^2}{(1 - \eta_-)^2} (\eta_+ - \eta_-). \tag{23}$$

For applying Eq. (23) to the elastic–cracked interface, we denote the quantities on the elastic and cracked sides of the interface by subscripts 1 and 2, respectively. The particle velocity and the radial stress on the elastic side of the interface are given by following equations:

$$v_1 = \frac{\partial u}{\partial t} = C_c \left[\bar{u}_1 - \xi_1 \frac{d\bar{u}_1}{d\xi_1} \right]_{\xi_1 = 1} = 3 C_c A \frac{(1 - \alpha^2)}{2\alpha^2}, \tag{24}$$

$$\sigma_1 = -\frac{A \rho C_e^2}{(1 - v)} \left[\frac{\alpha^3 (1 + v) - 3v\alpha^2 - (1 - 2v)}{\alpha^2} \right]. \tag{25}$$

The displacement solution derived in Eq. (8) along with the integration constants evaluated in Eq. (11) yields the stress distribution (and hence pressure) in the elastic region from Eqs. (3) and (4). The volumetric strain on the elastic side of the interface can be calculated by inserting the pressure thus calculated at $\xi_1 = 1$ into Eq. (22) as follows:

$$\eta_1 = -\left(\frac{3\sigma_f}{\frac{1}{2}\rho C_e^2} \right) \frac{\alpha^2 (\alpha - 1)(1 - v)}{[2\alpha^3 (1 + v) - 3\alpha^2 + (1 - 2v)]}. \tag{26}$$

Similarly, the volumetric strain on the cracked side of the interface can be calculated by inserting the displacement solution (Eqs. (16) and (19)) into the stress distribution solution (Eq. (13)), and finally evaluating the volumetric strain from Eq. (22) as follows:

$$\eta_2 = \frac{Y}{3K} \frac{(1 - \beta^2 \gamma^2)}{(1 - \beta^2)\gamma^2}. \tag{27}$$

Now evaluating the radial stress in the cracked region from either side of the discontinuity (from Eqs. (13), (16) and (19), and using the Hugoniot jump condition (Eq. (23)), the following relation between α and β is obtained.

$$\gamma^2 = \left(\frac{\alpha}{\beta} \frac{C_e}{C_{cr}} \right)^2 = \frac{Y(1 - \beta^2\gamma^2) \left[1 - \frac{\rho_0}{3K} \left(\frac{C_e - V_1}{1 - \eta_1} \right)^2 \right] + \sigma_1 \beta^2 \gamma^2 - \eta_1 \beta^2 \gamma^2 \rho_0 \left(\frac{C_e - V_1}{1 - \eta_1} \right)^2}{\sigma_1 - \eta_1 \rho_0 \left(\frac{C_e - V_1}{1 - \eta_1} \right)^2}. \tag{28}$$

The above relationship is not an implicit equation in γ, since the product $\beta\gamma$ is a function of α only.

6. Comminuted region

When the radial compressive stress in the cracked region, where the material has already failed in two orthogonal hoop directions, increases to the compressive strength of the material, it becomes granular or pulverized. A Mohr–Coulomb type material model is employed to define the material behavior of the

granular material. The granular material cannot support any shear in the absence of pressure, as observed by Rosenberg et al. (1987). Thus the cohesive strength is taken to be zero. There is a possibility that the level of comminution will vary with varying pressure, resulting in a non-linear pressure–shear behavior. We ignore this possible non-linearity, and assume that the shear strength increases linearly with the confining pressure. Later, we shall investigate the possibility of shear saturation. Denoting the constant of proportionality between pressure and shear by λ_1, for spherical symmetry

$$\frac{\sigma_r - \sigma_\theta}{2} = \lambda_1 \frac{\sigma_r + 2\sigma_\theta}{3}. \tag{29}$$

Using Eq. (29), the equation of motion, Eq. (2), reduces to

$$\frac{\partial \sigma_r}{\partial r} + 2\bar{\alpha}\frac{\sigma_r}{r} = -\rho\left(\frac{\partial v}{\partial t} + v\frac{\partial v}{\partial r}\right), \tag{30}$$

where $\bar{\alpha} = 6\lambda_1/(3 + 4\lambda_1)$. Employing the similarity transformations

$$\xi_3 = \frac{r}{Vt}, \quad \bar{u}_3 = \frac{u}{Vt} \quad \text{and} \quad U = \frac{v}{V}, \tag{31}$$

in the comminuted region, Eq. (30) becomes

$$\frac{\mathrm{d}\sigma_r}{\mathrm{d}\xi_3} + 2\bar{\alpha}\frac{\sigma_r}{\xi_3} = -\rho V^2 \frac{\mathrm{d}U}{\mathrm{d}\xi_3}(U - \xi_3). \tag{32}$$

The Mohr–Coulomb relation does not require any equation of state. However, to evaluate the convection quantities we need a relation between particle velocity and density. The equation of state of comminuted materials has not been established yet. Even if statistical homogeneity is assumed, the elastic moduli may be different from those of the intact material. Dilatancy and bulking due to comminution is counteracted by compaction due to presence of high pressure. Curran et al. (1993) observed that large scale dilatancy occurs only after the compressive stress has been removed. Hence, to first order, one may assume that the dilatancy and compaction cancel out each other. Ignoring any change in density in the comminuted region, the mass conservation equation (Eq. (1)) reduces to,

$$v = \frac{D_1}{r^2}, \tag{33}$$

where D_1 is the constant of integration. For a cavity being created in a continuous medium, with a constant cavity expansion velocity, $v(r = h) = V$. Thus, in terms of non-dimensional quantities, Eq. (33) becomes

$$U = \frac{1}{\xi_3^2}. \tag{34}$$

Inserting Eq. (34) into Eq. (32) and integrating once yields

$$\sigma_r = -\left(\frac{\rho V^2}{\xi_3^{2\bar{\alpha}}}\right)\left(-\frac{2}{2\bar{\alpha} - 4}\xi_3^{2\bar{\alpha}-4} + \frac{2}{2\bar{\alpha} - 1}\xi_3^{2\bar{\alpha}-1}\right) + \frac{D_2}{\xi_3^{2\bar{\alpha}}}, \tag{35}$$

where D_2 is the integration constant. The Hugoniot jump condition is invoked at the comminuted–cracked interface to evaluate D_2. By assumption, there is no dilatancy across the cracked–comminuted interface. Hence from Eqs. (20) and (21), there will be no jump in particle velocity or radial stress at this interface. But the density for this region is the same as that at the cracked–comminuted boundary. From Eqs. (17) and (22), the density is given by $\rho = \rho_0/(1 - Y/3K)$. Since $Y \ll K$, $\rho \sim \rho_0$. Now using the condition that the cracked material pulverizes when the radial stress equals the compressive strength, i.e., $\sigma_r|_{\xi_3=\delta} = Y$ (where $\delta \equiv C_\mathrm{p}/V$), and continuity of radial stress from the Hugoniot jump condition,

$$D_2 = Y\delta^{2\bar{\alpha}} + 2\rho_0 V^2\left(-\frac{1}{2(\bar{\alpha}-2)}\delta^{2\bar{\alpha}-4} + \frac{1}{2\bar{\alpha}-1}\delta^{2\bar{\alpha}-1}\right). \tag{36}$$

Finally, denoting the pressure at the cavity surface by P_c, the stress required to maintain the constant cavity expansion velocity for opening up a spherical cavity in a continuous ceramic medium is given by the following expression:

$$P_c \equiv \sigma_r|_{\xi_3=1} = Y\delta^{2\bar{\alpha}} + \rho_0 V^2\left(\frac{\delta^{2\bar{\alpha}-4}}{2-\bar{\alpha}} - \frac{2\delta^{2\bar{\alpha}-1}}{1-2\bar{\alpha}} + \frac{3}{(1-2\bar{\alpha})(2-\bar{\alpha})}\right). \tag{37}$$

The quantity δ needs to be related to α and β. Volume conservation in the incompressible comminuted zone, in terms of the non-dimensional quantities, is given by

$$(\xi_3 - \bar{u}_3)^3 = \xi_3^3 - 1. \tag{38}$$

Evaluating Eq. (38) at $\xi_3 = \delta$ and assuming that $\bar{u}_3(\xi_3 = \delta)$ is small,

$$\bar{u}_3(\xi_3 = \delta) = \frac{1}{3\delta^2}. \tag{39}$$

Continuity of displacement at the cracked–comminuted boundary is enforced by requiring that

$$\bar{u}_3(\xi_3 = \delta) = \delta\bar{u}_2(\xi_2 = 1). \tag{40}$$

Thus, from Eqs. (16), (39) and (40), the following relation between α, β and δ is obtained.

$$\delta^3 = \frac{1}{3\left[c_2 - c_1(1+\beta^2)\right]}. \tag{41}$$

To compute P_c as a function of the cavity expansion velocity, we adopt the following procedure. Starting with a given α, v_1 and η_1 are calculated from Eqs. (24) and (26), respectively. Then Eq. (28) is employed to compute β. Subsequently, the constants c_1 and c_2 are calculated from Eq. (19). Finally, δ is calculated from Eq. (41), from which P_c is calculated from Eq. (37).

7. Elastic-comminuted response

Numerical evaluations (shown later) indicate that the cracked zone disappears when the cavity expansion velocity increases beyond a certain value. Thereafter the material response is elastic–comminuted. In such a situation, the constant A in Eq. (8) needs to be re-evaluated using the boundary condition $\sigma_r(\xi_1 = 1) = Y$. Evaluation of Eq. (3) with Eqs. (6) and (8), along with the above boundary condition, yields

$$A = -\frac{Y(1-\nu)}{\rho_0 C_e^2}\left[\frac{\beta^2}{\beta^3(1+2\nu) - 3\nu\beta^2 - (1-2\nu)}\right]. \tag{42}$$

Also to evaluate δ, the boundary condition (40) must be replaced by

$$\bar{u}_3(\xi_3 = \delta) = \delta\bar{u}_1(\xi_1 = 1). \tag{43}$$

Evaluating Eqs. (43), (42), (39) and (8), the following relationship between β and δ is obtained.

$$\delta^3 = \frac{2\beta^2}{3A(2\beta^3 - 3\beta^2 + 1)} \tag{44}$$

The cavity expansion pressure is still given by Eq. (37).

8. Shear saturation in the failed material

Experiments (Rosenberg et al., 1987) suggest that the shear strength of the material immediately behind the shock wave in plate impact experiments saturates for shock pressures above the Hugoniot elastic limit (HEL). So far, we have modeled the comminuted material as a linear Mohr–Coulomb-type material. If the failed material saturates at a level $\sigma_r - \sigma_\theta = 2\tau$, the comminuted region can be divided into two sub-regions: a saturated region ($h < r < h'$) and a linear region ($h' < r < a$). From Eq. (29),

$$\sigma_r = \frac{2\tau}{\bar{\alpha}}. \tag{45}$$

The equation of motion for the saturated region becomes

$$\frac{\mathrm{d}\sigma_r}{\mathrm{d}\xi_3} + \frac{4\tau}{\xi_3} = -\rho V^2 \frac{\mathrm{d}U}{\mathrm{d}\xi_3}(U - \xi_3). \tag{46}$$

Integrating Eq. (46) with Eq. (34) from $r = h$ ($\xi_3 = 1$, $\sigma_r = 2\tau/\bar{\alpha}$) to $r = h'$ ($\xi_3 = \delta_1$, $\sigma_r = P_c$),

$$P_c = \frac{2\tau}{\bar{\alpha}} + 4\tau \ln \delta_1 + \frac{\rho V^2}{2}\left[3 + \frac{1}{\delta_1^4} - \frac{4}{\delta_1}\right]. \tag{47}$$

The equation of motion for the linear failed region is given by Eq. (32). Integrating this equation with the velocity distribution given by Eq. (33), from $r = h'(\xi_3 = \delta_1)$ to $r = a(\xi_3 = \delta)$ and recognizing that $\sigma_r(\xi_3 = \delta_1) = 2\tau/\bar{\alpha}$ and $\sigma_r(\xi_3 = \delta) = Y$, one obtains

$$Y\delta^{2\bar{\alpha}} - \frac{2\tau}{\bar{\alpha}}\delta_1^{2\bar{\alpha}} = 2\rho_0 V^2 \left[\frac{\delta^{2\bar{\alpha}-4} - \delta_1^{2\bar{\alpha}-4}}{2\bar{\alpha} - 4} - \frac{\delta^{2\bar{\alpha}-1} - \delta_1^{2\bar{\alpha}-1}}{2\bar{\alpha} - 1}\right]. \tag{48}$$

Thus for a given β, Eq. (44) is solved for δ. Eq. (48) is then iteratively solved to obtain δ_1, which is used in Eq. (47) to yield the cavity expansion pressure.

Finally, when the comminuted region is fully saturated (i.e. $\delta_1 = \delta$), the outer integration limit for Eq. (46) becomes $\sigma_r(\xi_3 = \delta) = Y$. Thus the expression for cavity expansion pressure becomes,

$$P_c = Y + 4\tau \ln \delta_1 + \frac{\rho V^2}{2}\left[3 + \frac{1}{\delta_1^4} - \frac{4}{\delta_1}\right]. \tag{49}$$

9. Results

As an application of the dynamic spherical cavity expansion analysis we have chosen Coors AD995 alumina ceramic for our study. The elastic constants for Coors AD995 alumina are calculated from the longitudinal and transverse wave speeds reported by Grady (1995) as $E = 373.14$ GPa, $K = 231.8$ GPa, $\rho = 3890$ kg/m. The quasi-static strength parameters as published by Coors are: compressive strength, $Y = 2.62$ GPa; and tensile strength $\sigma_f = 0.262$ GPa. Simha et al. (1995) measured the compressive strength of AD995 alumina from bar impact tests; it varied from 2.6 to 3 GPa. Bar impact tests of similar alumina give intermediate results, as shown by Brar et al. (1988) and Cosculleula (1992). Dandekar and Bartkowski (1993) measured the spall strength of this alumina as 0.462 GPa. Finally, based on Sairam and Cliftons (1994) experimental value of normal stress vs. shear stress coefficient of 0.2, $\lambda_l = 0.273$ (Satapathy and Bless, 1996).

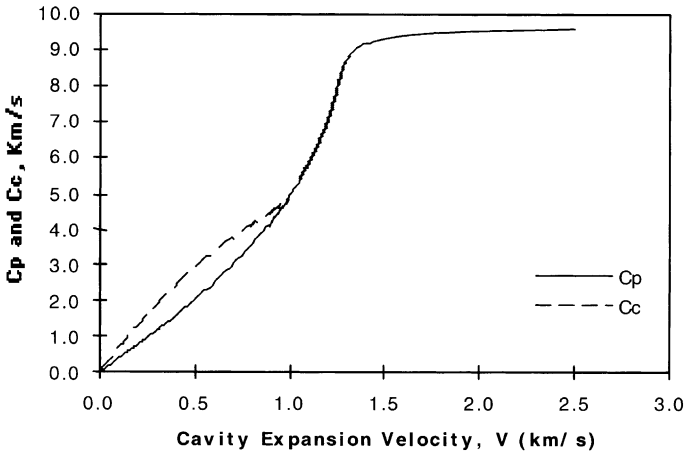

Fig. 2. Speeds of the comminuted and cracked zones.

Fig. 2 shows the expansion velocities of cracked and comminuted fronts for different cavity expansion velocities in AD995 ceramic. For a cavity expansion velocity of 980 m/s the cracked region disappears, i.e., $C_c = C_p = 4.9$ km/s. Thereafter the material response is elastic–comminuted. Similar observations were made by Forrestal and Tzou (1997) for dynamic cavity expansion in concrete. The speed of the comminuted zone becomes saturated at a level of 9.5 km/s, after a cavity expansion speed of about 1.5 km/s. This speed is lower than the dilatational elastic wave speed of about 10.5 km/s. Strassburger et al. (1994) had observed a saturation speed of about 9.5 km/s in end-on impact of alumina plates by cylindrical projectiles whose diameter was greater than the thickness of the target plates. Even though this experimental geometry was a plane stress configuration, the saturation limit speed of the failed zone seems to be similar to that found for spherical cavity expansion.

To adapt the dynamic cavity expansion pressure for modeling linear penetration, the penetration speed and penetration pressure must be suitably correlated to the cavity expansion speed and the cavity expansion pressure. To account for a non-uniform radial pressure distribution at the cavity wall, Goodier (1965) assumed a factor of $\cos\theta$ (θ is the angle from the axis of penetration) for the dynamic pressure variation on the penetration cavity wall. He then equated the pressure prevailing in the linear penetration process to the average cavity expansion pressure, which resulted in a multiplication factor of 2/3 for the averaged dynamic term in the force balance equation. On the other hand, Forrestal et al. (1995) adapted the dynamic spherical cavity expansion solution for metals by assuming a cosine variation in the normal component of the cavity expansion velocity. This assumption resulted in a multiplication factor of 1/2 for the averaged dynamic term in the force balance equation. Hydrocode simulations in CTH (Walker and Anderson, 1995) indeed indicate a spherical quality in the variation of velocity component around the cavity wall, using which Walker and Anderson introduced a velocity potential that resulted in a cosine variation for the particle velocity at the cavity wall. Even though Forrestal et al.'s approximation was introduced for rigid body penetration, and Walker–Anderson approximation was used for eroding penetration, both agree on the nature of particle velocity distribution at the cavity wall. We assume that the normal components of the penetration velocity exhibits a $\cos\theta$ variation i.e., it ranges from V at $\theta = 0$ to zero at $\theta = \pi/2$. The pressure variation resulting from this assumed velocity distribution is averaged over the hemi-spherical surface, i.e.,

$$\overline{P}_c = \langle P_c(V\cos\theta)\rangle = \frac{1}{2\pi r^2}\int_0^{2\pi}\int_0^{\frac{\pi}{2}} P_c(V\cos\theta)(r^2\sin\theta\,\mathrm{d}\theta\,\mathrm{d}\phi), \tag{50}$$

where the cavity expansion pressure function $P_c(V\cos\theta)$ acting on an elemental area of $r^2\sin\theta\,d\theta\,d\phi$, is derived in this paper. The pointed brackets and a bar over the variable are used to indicate averages. The average cavity expansion pressure so calculated is then compared to the penetration pressure. To assess the correctness of this approach, we compute the averages for eroding penetration into metal targets for which a well-established penetration equation (Tate, 1969) is available. The dynamic spherical cavity expansion pressure in an incompressible elastic–perfectly plastic material is given by (Hopkins, 1960)

$$P_c = \frac{2Y}{3}\left[1 + \ln\frac{2E}{3Y}\right] + \rho\left(a\frac{\partial^2 a}{\partial t^2} + \frac{3}{2}\left[\frac{\partial a}{\partial t}\right]^2\right). \tag{51}$$

Assuming a cosine variation of velocity, i.e. $\partial a/\partial t = V\cos\theta$ and steady state penetration ($\partial^2 a/\partial t^2 = 0$), inserting Eq. (51) in Eq. (50) results in

$$\overline{P}_c = \frac{2Y}{3}\left[1 + \ln\frac{2E}{3Y}\right] + \frac{1}{2}\rho V^2 \tag{52}$$

which exhibits identical velocity dependence in the target portion of the Tate equation.

The average cavity expansion pressures calculated from Eq. (50) for AD995 alumina ceramic are plotted in Fig. 3 for different levels of shear saturation in the comminuted region. The saturation values are indicated in the figure. The curves for no saturation cap yield the value of quasi-static cavity expansion pressure that was derived by Satapathy and Bless (1996) at zero cavity expansion velocity as a check for the numerical solution. Rosenberg et al.'s (1987) plate impact experiments suggested that the shear stress behind the shock wave saturates at about 2.7 GPa for AD85 ceramic. The material immediately behind the shock wave is unlikely to be totally damaged. Thus, the saturation level of the lower curve should be less than this value. In Fig. 3, the cavity expansion pressure is plotted for four different levels of saturation value and for $\lambda_1 = 0.273$. Experimental values from Subramanian and Bless (1995) for the interface pressure for a tungsten projectile penetrating a Coors-AD995 alumina ceramic for impact velocities up to 3.5 km/s (the abscissa in the plots are penetration velocity which are typically 0.5–0.7 times the impact velocity as measured experimentally) are also plotted in the same figure. Assuming that the specimen's finite size has not affected the experiments, the data exhibits closer agreement with the analytical solution for saturation stresses in the range of 1–1.5 GPa.

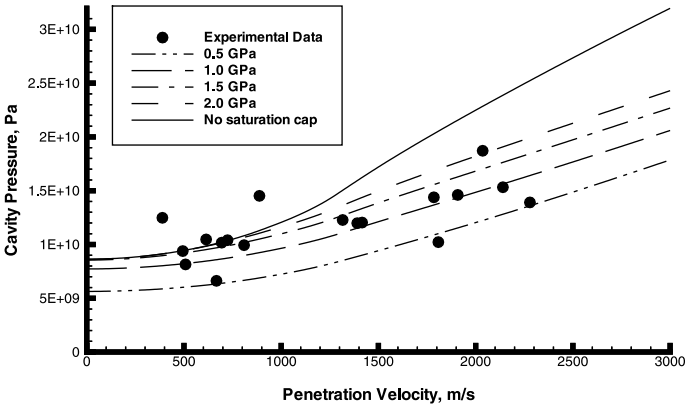

Fig. 3. Cavity expansion pressure vs. penetration velocity for different shear-saturation levels.

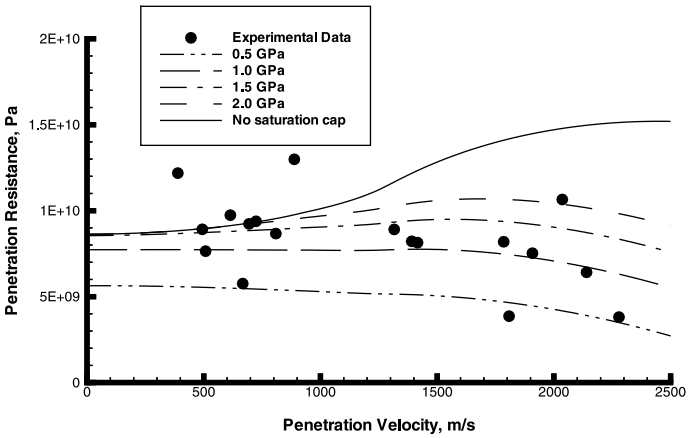

Fig. 4. Equivalent R_t vs. penetration velocity for different shear-saturation levels.

Tate equation (Tate, 1969) is frequently used to model high-velocity penetration into metal targets. This equation essentially is a one-dimensional modified Bernoulli equation, which equates the pressure exerted by the projectile to the pressure resisted by the target at the interface. Traditionally, penetration resistance of target materials is measured in terms of the target resistance, R_t in the Tate equation, where the inertial term is $0.5\rho U_p^2$. Fig. 4 shows the equivalent $(R_t = \langle P_c(V\cos\theta)\rangle - 0.5\rho U_p^2)$ calculated from Eq. (50) along with the experimental values obtained by Subramanian and Bless (1995). Again, the model with saturation stresses in the range of 1–1.5 GPa shows best agreement with the trend of the experimental data.

10. Conclusions

The dynamic cavity expansion solution shows that the cracked region disappears at high cavity expansion speeds as the comminuted region outruns the former. Thereafter at higher expansion speeds, the comminution region propagation speed saturates at a level slightly lower than the longitudinal wave speed. There is reasonable agreement between the theory and experiments on penetration pressure and penetration resistance in alumina ceramic. The cavity expansion model suggests that the quasi-static spherical cavity expansion pressure is a good approximation for the constant R_t term in the Tate equation for low-velocity penetration. Until a penetration velocity of about 2 km/s (for which the impact velocity is over 3 km/s) the penetration resistance decreases only slightly. Beyond this speed, the penetration resistance seems to exhibit potential sharp decrease. This behavior of ceramics is quite different from what is observed in penetration into RHA steel (Anderson et al., 1993). In the latter, the target resistance term decreases with increasing velocity. Thus, ceramics should offer better resistance against high-speed penetration.

Acknowledgements

This work was supported by the U.S. Army Research Laboratory (ARL) under contract DAA21-93-C-0101.

References

Anderson, C.E., Littlefield, D.L., Walker, J.D., 1993. Long rod penetration, target resistance, and hypervelocity impact. Int. J. Impact Engng. 14, 1–12.

Bishop, R.F., Hill, R., Mott, N.F., 1945. The theory of indentation and hardness tests. Proc. Phys. Soc. 57 (3), 147–159.

Brar, N., Bless, S.J., Rosenberg, Z., 1988. Brittle failure of ceramic rods under dynamic compression. J. de Physique C-C3 (9), 607–612.

Cosculleula, A., 1992. Plasticite, Engdommagements, et Ruptures des Alumines Sous Sollicitations Dynamiques Triaxiales: Influence de la Taille des Grains. Thesis, University of Bordeaux I.

Courant, R., Friedrichs, K.O., 1948. Supersonic Flow and Shock Waves. Springer, New York.

Curran, D.R., Seaman, L., Cooper, T., Shockey, D.A., 1993. Micromechanical model for comminution and granular flow of brittle material under high strain rate application to penetration of ceramic targets. Int. J. Impact Engng. 13 (1), 53–83.

Dandekar, D.P., Bartkowski, P., 1993. Shock response of AD995 alumina. In: Schmidt, S.C., et al. (Eds.), High Pressure Science and Technology. A.I.P., 1994. pp. 733–736.

Forrestal, M.J., 1986. Penetration into dry porous rock. Int. J. Solids Struct. 22 (12), 1485–1500.

Forrestal, M.J., Longcope, D.B., 1990. Target strength of ceramic materials for high-velocity penetration. J. Appl. Phys. 67, 3669–3672.

Forrestal, M.J., Luk, V.K., 1988. Dynamic spherical cavity-expansion in a compressible elastic–plastic solid. J. Appl. Mech. 55, 275–279.

Forrestal, M.J., Tzou, D.Y., 1997. A spherical cavity-expansion penetration model for concrete targets. Int. J. Solids Struct. 34 (31–32), 4127–4146.

Forrestal, M.J., Tzou, D.Y., Askari, E., Longcope, D.B., 1995. Penetration into ductile metal targets with rigid spherical-nose rods. Int. J. Impact Engng. 16 (5/6), 699–710.

Goodier, J.N., 1965. On the mechanics of indentation and cratering in solid targets of strain-hardening metal by impact of hard and soft spheres. Proceedings of the Seventh Symposium on Hypervelocity Impact III. AIAA, NY.

Grady, D.E., 1995. Dynamic properties of ceramic materials. Sandia Report, Sand 94-3266.UC-704.

Hopkins, H.G., 1960. Dynamic expansion of spherical cavities in metal. In: Sneddon, I.N., Hill, R. (Eds.), Progress in Solid Mechanics, vol. 1. North-Holland; Amsterdam.

Rosenberg, Z., Yaziv, D., Yeshurun, Y., Bless, S.J., 1987. Shear strength of shock-loaded alumina as determined with longitudinal and transverse manganin gauges. J. Appl. Phys. 62 (3), 1120–1122.

Sairam, S., Clifton R.J., 1994. Pressure-shear impact investigation of dynamic fragmentation and flow of ceramics. Proceedings of ASME Winter Annual Meeting.

Satapathy, S., Bless, S.J., 1996. Calculation of penetration resistance of brittle materials using spherical cavity expansion analysis. Mech. Mater. 23, 323–330.

Satapathy, S., Bless, S.J., 2000a. Deep punching PMMA. Experiment. Mech. 40 (1), 31–38.

Satapathy, S., Bless, S.J., 2000b. Cavity expansion resistance of brittle materials obeying a two-curve pressure-shear behavior. J. Appl. Phys. 88 (7), 4004–4012.

Satapathy, S., Bless, S., Ivanov, S.M., 1999. The effects of failure wave on penetration resistance of glass. Proceedings of the 18th International Symposium on Ballistics, San Antonio.

Simha, C.H., Bless, S.J., Brar, N.S., 1995. Dynamic failure of AD995 alumina. EXPLOMET'95, International Conference on Metallurgical and Material Application of Shock-wave and High-strain-rate Phenomena, EL Paso, TX.

Strassburger, E., Senf, H., Rothenäusler, 1994. Fracture propagation during impact in three types of ceramics. J. de Physique IV C8, 653–658.

Subramanian, R., Bless, S.J., 1995. Penetration of semi-infinite AD995 alumina targets by tungsten long rod penetrators from 1.5 to 3.5 km/s. Int. J. Impact Engng. 17, 807–816.

Tate, A., 1969. Further results in the theory of long rod penetration. J. Mech. Phys. Solids 17, 141–150.

Walker, J.D., Anderson, C.E., 1995. A time dependent model for long rod penetration. Int. J. Impact. Engng. 16 (1), 19–48.

Wright, S.C., Huang, Y., Fleck N.A, 1992. Deep penetration of polycarbonate by a cylindrical punch. Mech. Mat. 13, 277–284.